Published in JP Journal of Heat and Mass Transfer, 2018, vol. 15, Issue 3, pp.747 - 768, which should be cited to refer to this work.

DOI: http://dx.doi.org/10.17654/HM015030747

THERMODYNAMIC MODEL OF A PHASE-SHIFTING DEVICE OPERATING WITH A PHASE CHANGE MATERIAL

P. NIKKOLA[1]*, O. SARI[1], M. DESPONT[1], P. HAAS[2], P.W. EGOLF[3]

[1]Institute of Thermal Sciences and Engineering, University of Applied Sciences of Western Switzerland
Route de Cheseaux 1, CH 1401 Yverdon-les-Bains, Switzerland

[2] HEPIA/CMEFE, University of Applied Sciences of Western Switzerland
7, Route du Pont-Butin, CH 12 13 Petit-Lancy, Genève, Switzerland

[3] Institute of Theoretical Turbulence Research
Alte Wildeggerstrasse 5, CH 5702 Niederlenz, Switzerland

* Corresponding author: Petri Nikkola: petri@citycable.ch

ABSTRACT

A thermodynamic model of a "heat wave" phase shifter operating with phase change material (PCM) has been developed and experimentally investigated. The work started by building a physical model and developing numerical algorithms constructed to simulate its thermal behavior. Parameter studies reveal its operation characteristics and demonstrate a remaining potential for further improvements. This new phase shifter is a short term PCM heat storage device which uses the daily variation of the outside air temperature to indirectly cool the interior of a building. Besides sensible heat storage and phase shifting an important influence of the latent heat of the PCM is observed that originates from the high latent heat thermal inertia of the PCM. This latent heat greatly increases the heat storage capacity and, as a consequence, the phase shift of the "heat wave", compared to a device working solely with a material showing only a sensible heat capacity. To maximize the phase shifters efficiency it is important to operate the PCM in its full range between the solid (cold) and the liquid (hot) phase. Finally, a 45 % increase of the phase shift compared to only sensible heat storage could be achieved. In this article the derivation of this and similar results are outlined in detail.

Keywords: Phase change materials; PCM; continuous phase transition, phase shifter; Passive cooling.

1 INTRODUCTION

In ancient times, e.g. in the Roman empire, mainly the water/ice transition was used to cool and preserve food [1]. Then it was found that with additives, e.g. alcohol, glycol, etc., certain properties of water/ice may be positively influenced, e.g. its discontinuous first-order phase transition could be changed to a continuous phase change that instead of a point-wise transition now shows an enlarged melting temperature range [2]. Furthermore, the (mean) melting point could be shifted to a lower temperature. This then led to the discovery and development of further other phase change materials, that show the melting/freezing phenomenon also above the freezing point of water, which are roughly classified into organic materials (eutectics, mixtures, paraffin's, fatty acids, etc.) and inorganic materials (eutectics, mixtures, hydrated salts, etc.) [3]. The first category has the advantage of being non-corrosive and the

second one to usually be less flammable, which is an important feature demanded from PCM's introduced into building elements [4].

Today, phase change materials and their operation are studied by a broad community of scientists. *First*, there are the material scientists, involving chemists who are developing such materials with the practical objective of increasing the melting enthalpy under the boundary conditions of also maximizing the thermal conductivity of the material's solid and liquid phases [5]. Furthermore, sub cooling [6], which is a phenomenon that can occur, must be prevented. Then, cyclic stability [7] is demanded for practical engineering applications, when a safe operation during eventually thousands or even millions of cycles is imperative. In a daily storage application, there are approximately 300 times more cycles than in a yearly one, which, on the other hand, makes the first much more rentable.

Secondly, the phase transitions lead to complex mathematical problems as one is confronted with moving interfaces between the two phases (see e.g. [8]). If one phase is at least an order of magnitude less dense than the other, as e.g. in an air/water transition these problems are called free boundary-value problems [9]. The problem is that one is confronted with an interface for which one has boundary conditions (ev. in differential form) that need to be solved, however without initially knowing the position of this boundary, which itself is a part of the full solution. Such mathematically sophisticated problems are primarily studied by applied mathematicians, physicists and engineers. Physicists and mathematicians applied with success e.g. the Lagrange- and Hamilton principle [10] to solve such problems, whereas engineers benefited much from a method called the enthalpy method [11] to tackle such complex problems (the model applied in this article is a modified enthalpy method).

Thirdly, engineers and architects apply PCM's in technical systems and building applications. From hundreds of PCM possibilities they usually take a choice out of a smaller group of materials that are sufficiently stable and have over the decades proven to be enough reliable for a practical application (e.g. calcium chloride hexahydrate, sodium carbonate, etc.). These engineers build laboratory set-ups and perform measurements (see for example [12]). Furthermore, they also model PCM systems to study their behavior and compare theoretical with experimental results. In this way, general knowledge can be extracted to optimize the systems, so that minimum charging and discharging times can be obtained that are finely tuned to their specific applications. The work presented in this article belongs into this category and has as its specialty a focus on the phase shifting effect of temperature profiles from day to night in heating and from night to day in cooling applications of buildings.

The article shows the in the following described structure. In Sect. 2 the development of the thermodynamic model is described and it presents the complete mathematical formulation. In Sect. 3 numerical results are compared with analytical ones. In Sect. 4 the bench mark test is presented and described, and its characterizing parameters are listed. Sect. 5 is devoted to the characteristics of the applied PCM. In Sect. 6 experiments with the phase shifter and its comparison with numerical results are outlined. Finally, in Sect. 7 the article is complemented by some conclusions and an outlook.

2 THE THERMODYNAMIC MODEL

In this section the model geometry, the equations and the solving method as well as the implementation method of the model are described in detail. Then, also a set of numerical solutions of the thermodynamic model is presented. Some calculations were intentionally

kept simple to facilitate comparisons of the numerical solutions with well-known analytical results. After these tests the complexity was increased and more practical results were attempted. We also decided to provide short information on the convergence tests and experiences, which are results that are valuable to other scientists confronted with nonlinear numerical diffusion modeling. The thermodynamic model basically consists of two main components: 1) the solid or/and liquid PCM domain and the channel domain filled by (moving) air. These two basic elements are separated by an impermeable wall, however, they are coupled by a heat flow through this material-impermeable wall. Thermodynamically, such a system is called a 'closed system'. The coupling by heat transfer takes place at the air-PCM boundary of the channel where a convective heat exchange takes place. Here, the PCM container wall is assumed to show a high diffusivity and small thickness, so that its thermal resistance may be neglected.

The air flow in the channel is approximated as a standard incompressible *1-d* thermal flow whereas the PCM temperature is solved with a nonlinear heat diffusion model.

2.1 Model geometry

A Cartesian geometry is sufficient to simulate the thermodynamic behaviour of the phase shifter which is mounted together by rectangular plates containing the PCM and a single, also rectangular, air containing channel. The air channel is surrounded by the plate-like PCM modules on the top as shown in Fig. 1.

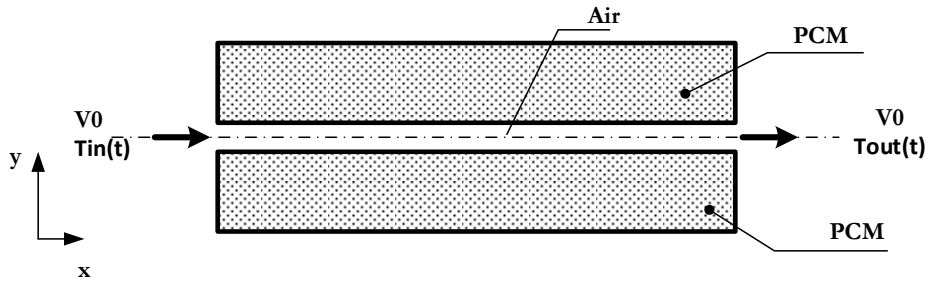

Figure 1. Model geometry. The horizontal air channel is located in the middle between two PCMs containing rectangular plates.

The usually time-dependent convective heat transport is modelled in the downstream direction (in x-direction) for bins of width Δx. The nonlinear diffusion process in the PCM is spatially modelled in two dimensions (x- and y–directions). However, this process is not taken into consideration in the z-direction, perpendicular to the x- and y-direction. In this direction we actually assume infinitely extended plates.

2.2 Model equations

For an extensive review of the modeling of PCM's see e.g. Ref. [13]. Solidification and melting constitute mathematically a classical nonlinear moving boundary value problem. In the basic and ideal situation, two modeled domains constitute of a separate component each, which are a solid and a liquid phase, respectively, separated by an infinitely thin interface. If heat fluxes occur this interface moves and if the solid and the liquid show different densities,

then internal liquid flows are initiated and the solution becomes more challenging, because the chosen melting model must also be incorporated to the coupled continuity and momentum equations (Navier-Stokes equations). Numerous studies have shown that for engineering applications a constant density (ideally being the average of the density of the solid and liquid phase) usually lead to sufficient reliable results (see e.g. Ref. [12]). Therefore, the boundary position as a function of time and space needs to be determined in the context of solving the entire problem. For a half-infinite plate there exist analytical solutions, whereas for complexer geometries numerical calculations must be performed.

Let us first briefly explain the analytical method and its limitation. A simple situation showing solidification and melting of pure phases is called the Stefan problem [14].

Only the one-phase Stefan problem is even simpler. In this special case the liquid phase is precisely at its solidification temperature or the solid phase is exactly at its melting temperature. A jump to a constant temperature boundary condition is imposed on one side of the one-dimensional infinitely extended slab. The solution of the problem then consists of the entire spatial temperature distribution for all times and, additionally, of the location of the solidification, respectively, melting front as a function of time. In this example, both phases show the constant phase-change temperature.

The solution of the two-phase Stefan problem is also called the Neumann solution of the Stefan problem [15]. In this case the temperatures of the two components may differ from the phase change temperature. The solution of the Neumann problem is rich as it contains not only the time dependent temperature profiles of the solid and liquid phases, but also the location of the interface as a function of time. Usually a jump temperature boundary condition is applied to the half-infinite slab. Not so much known is that there exists an analytical solution for the two-phase Stefan problem with a convection boundary condition [16]. The main limitations of the basic and modified Stefan problems with their analytical solutions are:

- A semi-infinite slab geometry is used. Therefore, only a single boundary can be modelled. No PCM of a certain thickness can be reasonably modelled by such a crude approximation.
- The initial temperature profile is assumed to be uniform. We will experience that this is not the case in the problem dealt with in this article.

For these reasons analytical solutions are not the method to pursue. Nevertheless, the Neumann solution can be used as an ideal test example for our numerical model that can solve more general cases. Naturally, that does not prove correctness in all cases, but it is surely a method to give improved confidence.

For the modeling of the nonlinear heat diffusion process in the PCM, we have chosen the Continuous-Properties Model (CPM) of Egolf and Manz [17]. In this solid model the evolution of the temperature profile $T_s(t,y)$ of the PCM is governed by a generalized nonlinear heat diffusion equation with effective (temperature dependent) physical properties

$$\frac{\partial T_s(t,y)}{\partial t} = \alpha(T_s)\frac{\partial^2 T_s}{\partial y^2} + b(T_s)\left(\frac{\partial T_s}{\partial y}\right)^2 . \qquad (1)$$

The first two terms with the coefficent α comprise the usual heat diffusion equation. However, here α is not constant; it is defined by

$$\alpha(T_s) = \frac{k_s(T_s)}{\rho_s c_s(T_s)}, \tag{2}$$

where k_s is the thermal conductivity of the PCM, ρ_s is the density assumed to be constant, and c_s is the specific heat capacity. In the nonlinear term the coefficient b is given by

$$b(T_s) = \frac{dk_s/dT_s}{\rho_s c_s(T_s)}. \tag{3}$$

The boundary condition on the outer edge of the PCM domain $y = y_b$ is

$$\frac{\partial T_s}{\partial y} = \Big|_{y=y_b} 0. \tag{4}$$

For the air channel the model of Hollmüller [18] is applied in Cartesian coordinates. The air temperature $T_a(t,x)$ evolves as

$$\frac{\partial T_a(t,x)}{\partial t} = -v_a \frac{\partial T_a}{\partial x} + \frac{L_w h_c}{c_a \rho_a A_c}\left(T_s|_{y=y_0} - T_a\right). \tag{5}$$

In Eq. (5) v_a is the air axial velocity, c_a is the specific heat capacity, ρ_a the constant air density, and A_c the cross section of the air channel. The wetted perimeter is $L_w = 2w_a$, where w_a is the channel width. The convective heat transfer coefficient is given by the relation

$$h_c = \frac{k_a Nu}{D_H}, \tag{6}$$

where k_a is the thermal conductivity of the air, $D_H = 2w_a h_a/(w_a+h_a)$ is the hydraulic diameter of the rectangular channel of width w_a and height h_a and Nu is the abbreviation for the dimensionless Nusselt number for laminar flow. For an infinitely extended small slit rectangular channel this number is: $Nu=7$. The standard expression for the laminar flow pressure gradient is used even though it is generally so small that the pressure drop can be neglected for air speed less than 1 m/s, which is typical for our numerical simulations and experiments. The boundary condition at the air inlet and at the left outer edge of the PCM is

$$T_a(t, x = 0) = T_{in}(t) \tag{7}$$

Finally, Eq. (1) (PCM) and Eq. (5) (air) are coupled by convection at the air-PCM interface by

$$k_s \frac{\partial T_s}{\partial y}\Big|_{t,x,y_0} = h_c\left(T_s(t,y_o) - T_a(t,x)\right), \quad y = y_o. \tag{8}$$

The basic diffusion equation (1) is a nonlinear partial differential equation, even in the limit when the second nonlinear term is negligible. This is so, because $\alpha(T_s)$ is temperature dependent. Because of the high mathematical complexity an iterative method is required to solve for the temperature distribution within the PCM domain. The usual Newton method with finite differences discretization was employed. The discretized problem was linearized and the corresponding Jacobian formed. Inverting the Jacobian delivers the solution for the linearized problem. With this, the full solution is constructed by introducing a perturbation to this initial solution, linearizing the boundary value problem in the perturbed temperature and then integrating. The process is repeated until the correction of the linearized solution to the full solution is negligibly small. The solver is written as a Matlab script and uses the fast

Matlab sparse matrix formulation. The Jacobian inversion is performed by applying the Matlab symbol '\'. Backward discretization is applied for both, the spatial and time discretization. The backward time discretization has the advantage to rest stable independently of the chosen spatial and temporal step size. To calculate the temperature distribution in the air channel a backward finite difference scheme is used. Because the backward spatial discretization method is applied, and Eq. (5) does not contain any nonlinear terms, this equation can be solved throughout the air channel. However, Eq. (5) is fully linear, because the air characteristic density and speed are assumed to be constant. As a consequence, the application of the Newton iteration method is not required for the total air domain. Inverting the sparse finite differences coefficient matrix is sufficient to find the final solution.

2.3 Quantification of the phase shift

The phase-shift between the inlet air temperature and the outlet air temperature φ is calculated as follows. The phase of a near to sinusoidal function f can be found as

$$\varphi = 2\pi - tan^{-1}\left(\frac{C_f}{S_f}\right), \tag{9}$$

where the functions C_f and S_f are

$$c_f = \int_0^{2\pi} cos\left(\alpha \hat{f}(\alpha)\right) d\alpha \tag{10-a}$$

$$s_f = \int_0^{2\pi} sin\left(\alpha \hat{f}(\alpha)\right) d\alpha\,, \tag{10-b}$$

and $\hat{f}$ is the fluctuating component (zero mean value) of the original function f normalized so that $\int_0^{2\pi} \left|\hat{f}(\alpha)\right| d\alpha = 4$. The phase shift ϕ is then the difference between the phases of the inlet and outlet temperature signals

$$\phi = \varphi_{outlet} - \varphi_{inlet} \tag{11}$$

The transmission Γ is the ratio of the integrals (10a,b), evaluated over a single period, of the absolute value of the fluctuating components of the outlet and inlet air temperatures. This serves as the main characteristic parameter of the evaluation method of the system.

2.4 Material coefficients

The material properties of the PCM, namely the specific enthalpy and the thermal conductivity are modeled with two mainly antisymmetric exponential functions which are continuous at the phase change temperature T_m, as explained in detail in Ref. [18]. The *S*-shape transitions of the physical properties, as e.g. the specific enthalpy, the thermal conductivity, etc. are modeled by a convex exponential function (with characteristic temperature constant τ_1) to the left-hand low-temperature side of the mean melting/freezing temperature T_m and by a concave exponential function (with characteristic temperature constant τ_2) to the right-hand high-temperature side. Thereby, the total width of the mushy region can be exactly defined by the formulae $\tau = \tau_1 + \tau_2$. For further details, please consult Ref. [17].

3 COMPARISION OF NUMERICAL WITH ANALYTICAL SOLUTIONS

In this section the solutions of the simulations of the numerical PCM model are compared to analytical solutions of the Neumann problem (see Sect. 2.2). In Fig. 2 the numerical and analytical solutions of the Neumann problem for solidification are shown.

The PCM calcium chloride hexa hydrate ($CaCl_2 \cdot 6H_2$) is initially in its liquid phase at a temperature of 32°C, which is clearly above the phase change temperature of 27°C. A discontinues cooling jump, defined by a final temperature of 22°C, is imposed at t=0 on the left boundary located at x=0. The temperature profiles are shown for solidification for different values of τ after 10 h. It can be observed that the numerical solution for $\tau = 1$ K is very close to the analytical Neumann solution (see Fig. 2 on the left). Therefore, we can assume that with even smaller τ's it would fully converge toward the analytical result. As expected a higher deviation from Neumann's solution occurs, if the mushy region is chosen to be five times larger, namely with $\tau = 5$ K. An interesting finding is that the solidification front propagation speed does not depend considerably on τ (see Fig. 2 on the right).

In analogy to Fig. 2, in Fig. 3 the melting process is shown. Here the PCM is initially in its solid state at 22 °C, which is below the phase change temperature 27°C. In this case the discontinuous heating jump is performed at x = 0 and t = 0 s from 22 °C instantaneously to

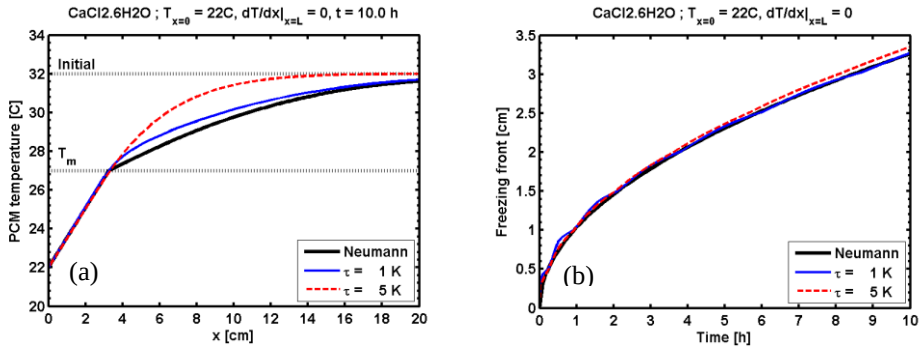

Figure 2. The two panels compare numerical with Neumann analytical solutions in a solidification process: (a) temperature profiles (b) position of the melting front as a function of time. The black line is the analytic Neumann solution, the blue line the model prediction with a mushy zone of width $\tau = 1$ K; the red dashed line shows the result with a mushy region width of $\tau = 5$ K.

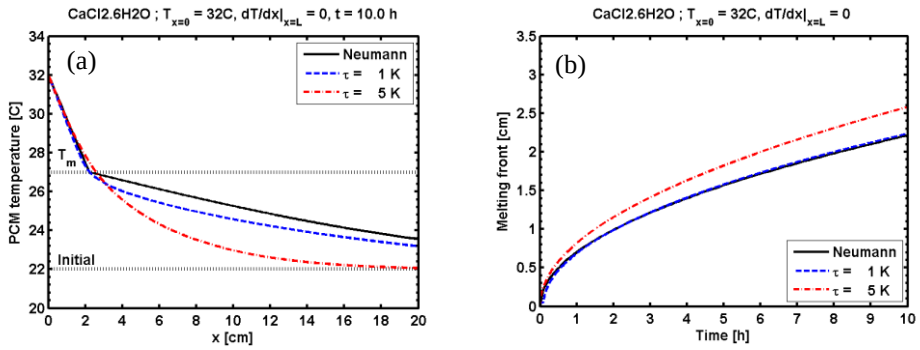

Figure 3. As Fig. 2, but here for the freezing process.

32 °C. It is observed that the temperature profile as a function of τ exhibits a similar behavior as that in the melting case. The front propagation speed is generally lower than in the solidification process. The explanation for this is the smaller diffusivity of the liquid phase as compared to that of the solid one. However, the melting front propagates somewhat faster with a larger mushy region width. This is easily understood as a physically consistent result, because the mushy region is a mixture of the liquid and solid phase. The case with $\tau = 5$ K shows to the front more solid concentration in its mushy region and, therefore, has a higher diffusivity.

4 THE TEST BENCH

A bench mark test was constructed in order to weigh the model predictions. It is a sandwich geometry of three Alba®Balance plates and two air channels between the plates. The device length is 1 m and the width 0.5 m. The air channel height is 6 mm and the Alba balance plate thickness 25 mm. The device is surrounded by polystyrene plates of 5 cm thickness and packed into a wooden box, see Fig 4. Panel (a) shows the white wooden box containing the PCM plates in the middle and the tapered air inlet on the right. Panel (b) shows the thermocouples attached to the PCM plate surface. A honeycomb sheet at the air inlet can also be seen on the left-hand side.

The temperature of the inlet air and the air speed can be controlled. Typically, the air speed was v = 0.4 m/s and the air inlet temperature between 20 °C and 31 °C so that the phase change temperature, T_m , was within the maximum possible inlet temperature difference. The device is equipped with nine thermocouples, two positioned in the air stream and seven fixed on the PCM plate surfaces with downstream positions as listed in Table 1. Laterally, the thermocouples were mounted in the middle of the plates, namely at. $w_a/2$ = 0.25 m.

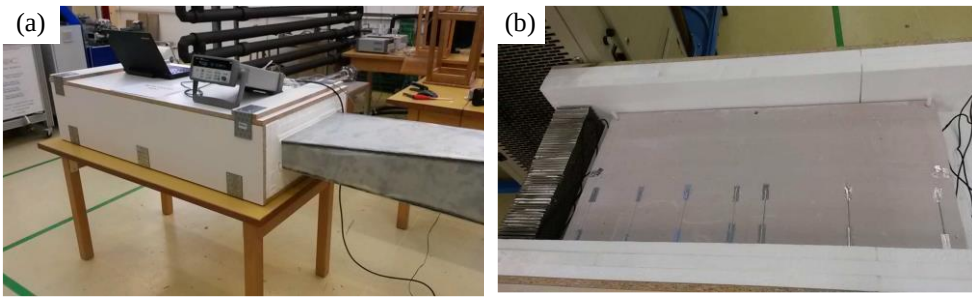

Figure 4. Two photographs of the bench mark arrangement: (a) general overview, (b) picture of the surface of a PCM plate.

Table 1. Positions of the thermocouples in axial positions. The temperature values of the bold thermocouples are shown in the figures of Sect. 6.

	Name	Type	Axial location [mm]
Air inlet	**Ta1**	**K**	**0**
Air outlet	Ta2	K	1000
PCM surface	**Ts1**	**PT100**	**40**
PCM surface	Ts2	PT100	180
PCM surface	Ts3	PT100	320
PCM surface	**Ts4**	**PT100**	**460**
PCM surface	Ts5	PT100	540
PCM surface	Ts6	PT100	750
PCM surface	**Ts7**	**PT100**	**960**

5 THERMAL CHARACTERISTICS OF THE PCM

The PCM Alba®Balance plates use Micronal® PCM produced by BASF (DS 5039 X). The Micronal® material was encapsulated into polymer microcapsules. The characteristics of the Alba®Balance plates are listed in Table 2.

Table 2. Alba®Balance thermal characteristics.
(http://ch.rigips.de/download/pdb_alba_balance_fr.pdf)

Phase change temperature	T_m	23 °C	Specific heat	c_s	1.16 kJ kg^{-1} K^{-1}
Latent heat	h_{12}	13 kJ kg^{-1}	Heat conductivity	k_s	0.27 W m^{-1} K^{-1}
Density	ρ_s	900 kg m^{-3}	Mushy region width	τ	1.5 K - 4.5 K

Data of a measurement of the mushy region width for DS 5039 X can be found in Ref. [19]. In Fig. 5 the measured values of the specific heat $c_p(T)$ are shown by quadratic pointers that are linearly fitted by the black curve. They show a large continuous mushy region below the mean melting temperature, which is characterized by the position of the peak of the specific heat, and a rather narrow one above. In comparison two calculated piecewise exponential curves, as explained in Sect. 2.3, are presented for mushy regions characterized by a total widths of τ = 1.5 K (blue line) and τ = 4.5 K (red line). To take the asymmetry of the measured mushy region into consideration, the following partitions were taken as best fits a) $\tau = \tau_1 + \tau_2$ = 1.0 K + 0.5 K =1.5 K (blue case) and $\tau = \tau_1 + \tau_2$ = 4.0 K + 0.5 K =4.5 K (red case). By studying this figure, it is evident that the case with smaller width of the mushy region fits the measurements better in the peak region between 21 °C and 23 °C, whereas that with the larger width fits exceptionally well at low temperatures, e.g. when T < 21°C. Finally, we have chosen the case with the larger width. By this we also benefited by a higher numerical stability and a lower calculation (CPU) time given by the possibility of choosing a spatially wider discretization scheme.

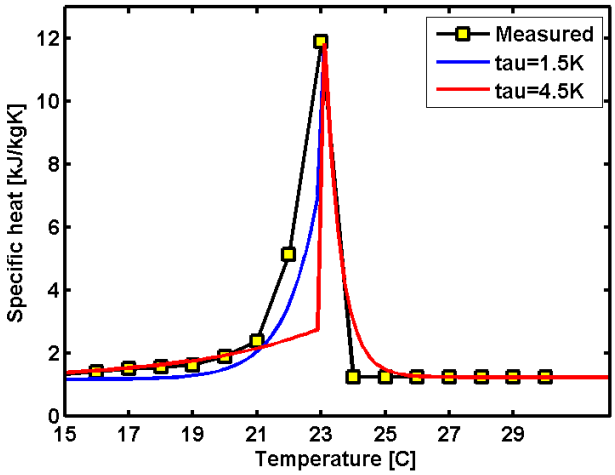

Figure 5. Measured specific heat of DS 5039 X (black line with square symbols) [19], and theoretical determined specific heat composed with two piecewise exponential functions (see Section 2.3) with τ=1.5 K (blue line) and with τ=4.5 K (red line).

6 COMPARISON WITH MEASUREMENTS

The numerical model results have been compared with measurements made with the bench mark test as described in Sect. 5. We conjecture and accept the fact, that by symmetry each internal air channel surface is actually only related to a PCM body of half the thickness of a plate. Furthermore, the two side air channels, because of their lack of symmetry, experience here the influence to only one side of a single plate. This is corrected by an approximation given by the introduction of an effective plate thickness,

$$h_{s,eff} = \frac{1}{2}\left(h_s + \frac{h_s}{N_a}\right) = \left(\frac{1+N_a}{2N_a}\right) h_{s,} \tag{12}$$

where N_a denotes the total number of plates. Since the device at HEIG-VD has two air channels the effective PCM plate thickness is

$$h_{s,eff} = \frac{3}{4} h_s = 18.75\ mm$$

The numerical results of the air temperature in the channel are shown in Fig. 6. The air inlet temperature (see Table 1: Ta1) is presented by the black line and the three surface temperatures measured by the thermocouples fixed to the surface of the plates (see Table 1: Ts1, Ts4 and Ts7) are presented by blue, green and red colored lines. In Panel (a) is shown the comparison of theoretical results obtained with a mushy domain width of τ = 1.5 K and with measurements. Panel (b) shows the analogous results for τ = 4.5 K. In both figures the solid lines are measured values and the dashed lines are the model results. Both model results agree relatively well with the measured values. The case characterized by τ = 1.5 K seems to better predict the rise of the temperature at t < 15 h, especially close to the outlet (red line), whereas the second case, characterized by τ = 4.5 K, shows good agreement at all axial positions when the temperature decreases for t > 15 h. We conclude that (i) the simulation results are in a good agreement with the measured values, (ii) the model is not very sensitive to the chosen τ value, and (iii) in order to better reproduce the experimental results a more detailed presentation of the material thermal characteristics of the model would be required, i.e., use of a piecewise fit with numerous (n > 2) functions rather than n = 2, as in the current model.

In Fig. 7 the surface temperature contours on the plate are presented. The horizontal axis is the time in hours and the vertical axis is the axial distance from the air inlet. In Panel (a) the measured temperatures are presented. One can clearly see how the temperature maximum is delayed by a time of 10 h at the inlet to about 15h at the outlet. The numerically calculated temperature values are presented in Panel (b). They have practically identical behavior and show a comparable phase shift of the temperature. Simulations results using standard Alba plates without PCM are shown in Panel (c); they show quite different evolution scenarios of the temperatures.

Figure 8(a) shows a typical model prediction of a case with a sinusoidal inlet air temperature with a mean temperature of 23°C and an amplitude of 8°C. The length of the period is 24 h. The air speed was v_a = 1m s^{-1}. The length and width of the device was 3.0 m and 0.5 m, respectively. The channel and PCM geometry were as listed in Table 2. Two periods were calculated because the first period is an initialization period containing small transients. This can be seen, because during the second period the outlet temperature is different from the values of the first period. A third period leads to a practically identical profile as the second one. This is due to the initial conditions, namely the fact that at the beginning the radial PCM temperature profiles were equal at all axial positions.

With these parameters the model predicts a phase shift of φ = 7.6 hours and a transmission of Γ = 45%. The calculation time for the 3 m long device was about 15 min on a 2.26 GHz Intel Xeon CPU.

Panel (b) presents the numerical simulation results of the device equipped with standard Alba panels containing no PCM. Thus, only the sensible heat creates a temperature phase shift. It is observed that the outlet air temperature has exactly the same sinusoidal shape

as the inlet temperature. The typical ‘shoulders’, which visualize a stabilization of the temperature in the mushy region, in the temperature evolution graphics in the environment of the phase change temperature, T_m = 23°C, are absent.

In the case with only sensible heat storage, the phase shift is φ = 4.2 hours and the transmission is approximately Γ=85 %. Thus, the PCM increases the phase shift by more than three hours, namely from 4.2 to 7.6 hours.

(a)

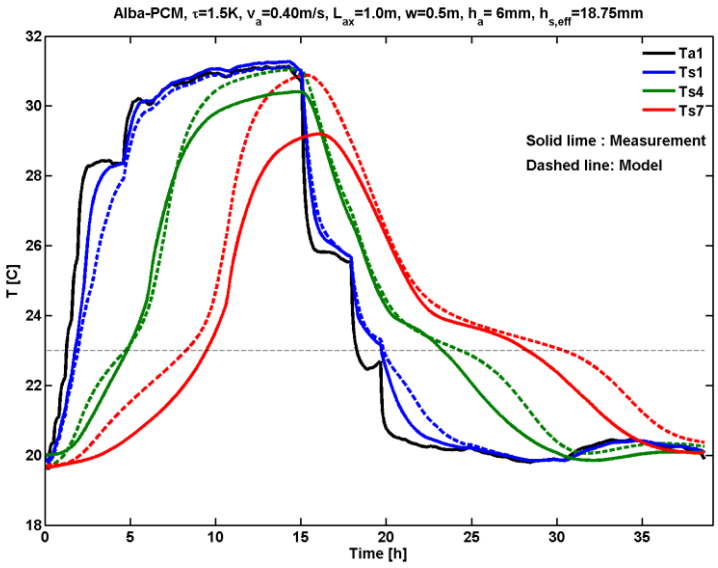

(b)

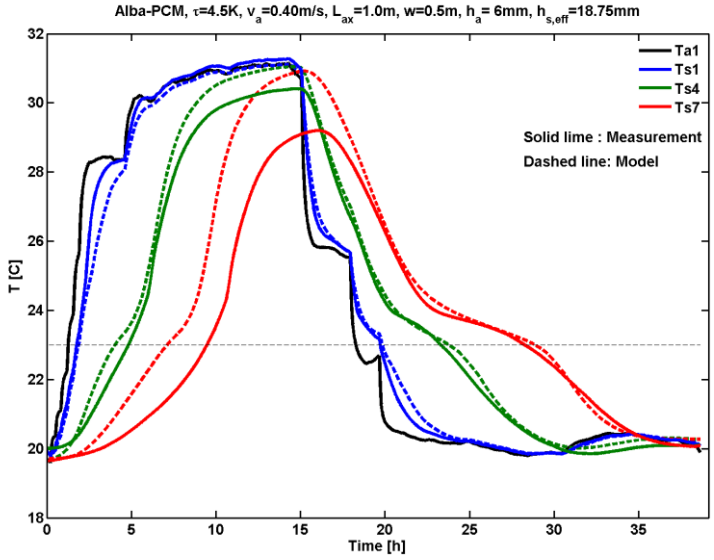

Figure 6. Comparison of measured (solid lines) and calculated (dashed lines) temperature evolutions of the air at the inlet and in the PCM plates of the bench mark test: (a) τ = 1.5 K (b) τ = 4.5 K.

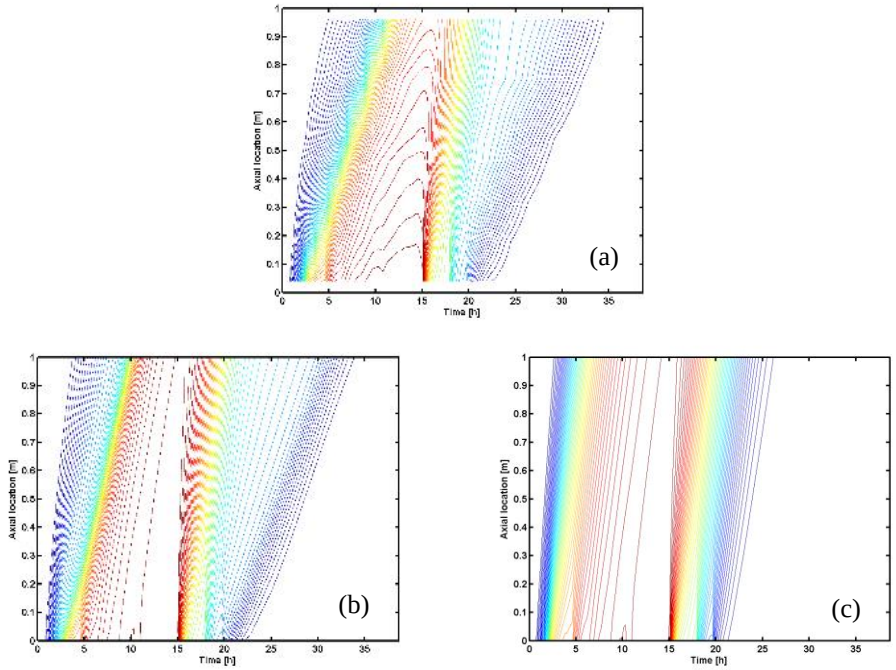

Figure 7. Temperature contour plots of the measurements in Fig. 6. (a): Measured values with Alba®Balance. (b) Simulation values with Alba®Balance. (c) Simulation values with standard Alba plates without PCM. The contour lines correspond to the same temperature in each figure, the minimum temperature being 20.5°C and the maximum 31°C. The spacing between contour lines is 0.2°C.

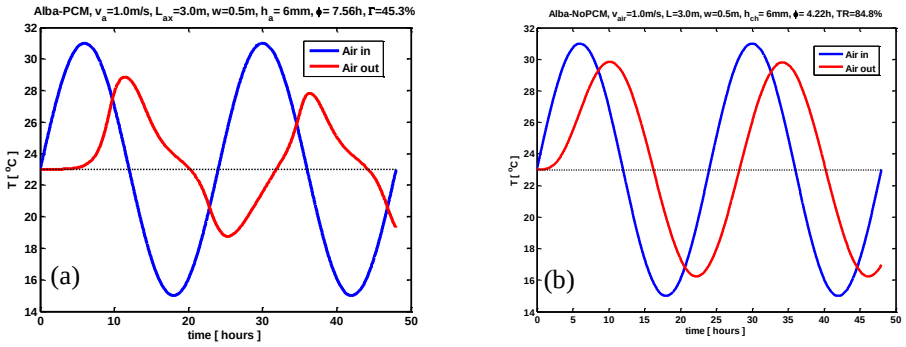

Figure 8. Simulations of air outlet temperature (red line) as a result of a sinusoidal inlet temperature signal (blue line): (a) with Alba®Balance PCM plates with a phase change temperature of 23°C; (b) with standard Alba plates without PCM.

7 CONCLUSIONS AND OUTLOOK

By the term ‘heat wave’ we mean a periodically excited temperature at a boundary that is also periodically diffusing into a sensible or/and latent heat material. Notice that the physical problem contains no wave equation, as it e.g. occurs in a superfluid with real entropy, respectively heat waves! In the first case there is no deformation, whereas in the second an influence by temperature stabilization slightly deforms the periodical signal. Thereby, a device was built, called ‘heat wave shifter’. It is a test device in our laboratory which delivers exact experimental data. These data were applied to evaluate a complex numerical model solving heat diffusion in a PCM, which is described by a parabolic nonlinear heat diffusion equation coupled to a convective fluid- and thermodynamic physical model. The entire solving process is described in this article; it is of iterative nature. Good agreement between experimental and numerical results could be obtained. Furthermore, it was shown that a phase shift of approximately eight hours can easily be realized, which is nearly the double time difference compared with a “heat wave” shifter working only with sensible heat transfer and storage.

In future work, we propose to more systematically investigate the wave shifter by designing new experiments. With the help of extensive numerical parameter variations design rules for building engineers and architects could be worked out and published for a support of new renewable, sustainable and energy efficient heating and cooling systems.

ACKNOWLEDGEMENTS

The authors are grateful to Kolumban Hutter (ETHZ), who suggested some linguistic amendments.

REFERENCES

[1] Hansen, T.M., Kauffeld, M., Sari, O., Egolf, P.W. Pasche, F., *Research, Development and Applications of Ice Slurry in Europe - From Ancient Rome to Modern Technologies.* Proceedings of the Fourth Workshop on Ice Slurries of the International Institute of Refrigeration in Paris, 1-12, 12-13 November, Osaka, Japan, 2001.

[2] Robinson R.A., Bower, V.E., *Properties of Aqueous Mixtures of Pure Salts. Thermodynamics of the Ternary System: Water-Sodium Chloride-Calcium Chloride at 25 °C.* Journal of Research of the National Bureau of Standards, A, Physics and Chemistry Vol. **70A**, No. 4, July- August, 1966.

[3] Zalba, B., Marin, J.M., Cabeza, L.F., Mehling, H., Review on thermal energy storage with phase change materials, heat transfer analysis and applications, *Appl. Therm. Eng.* 23, 251-283, 2003.

[4] Tyagi, V.V., Buddhi, D., PCM thermal storage in buildings: A state of the art. *Renewable Sustainable Energy Rev.* **11**, 1146-1166, 2007.

[5] Lane, G.A., *Solar Heat Storage: Latent Heat Material – Latent Heat Materials*, Volume II, CRC Press Florida, 1983.

[6] Solomon, G.R., Karthikeyan, S., Velraj, R., Sub cooling of PCM due to various effects during solidification in a vertical concentric tube thermal storage unit. *Appl. Therm. Eng.* **52** (2), 505-511, 2013.

[7] Han, L., Xie, S., Ma, G., Sun, J., Jia, Y., Jing, Y., Test and improvement of the cyclic stability of oxalic acid dehydrate for thermal energy storage. *Thermochimica Acta* 645, 24-30, 2016.

[8] Ying, L. Three Dimensional Interface Problems for Elliptic Equations. *Chinese Annals of Mathematics*, Series B, 28B (4), 441-452, DOI: 10.1007/s11401-005-0334-2.

[9] Hoffman, K.H., Sprekels, J., *Free Boundary Value Problems*, International Series of Numerical Mathematics, Birkhäuser Edition, Basel, Switzerland, ISBN 978-3-7643-24 74-2, 1990.

[10] Salmon, R., Hamiltonian Fluid Mechanics. *Ann. Rev. Fluid Mech*. **20**, 225–256. Bibcode: 1988AnRFM..20..225S. doi:10.1146/annurev.fl.20.010188.001301, 1988.

[11] Voller, V.R., Cross, M., Markatos, N.C., An enthalpy method for convective/diffusive phase change, *Num. Meth. Eng.* 24 (1), 271-284.

[12] Egolf, P.W., Manz, H., Furter, R., Odermatt, A., Frei, B., Lüscher, H., *The Continuous-properties Model and Colour-visualized Experiments of a Water Storage Tank Containing Spherical PCM Capsules*. Proceedings of the Sixth International Conference on Thermal Energy Storage, 22-25 August, Helsinki University of Technology, Espoo, Finland, Volume 2, 495-502, 1994.

[13] Huy H. & Argyropoulos S.A., Mathematical modelling of solidification and melting: a review. *Modelling Simul. Mater. Sci. Eng.*, **4**, pp. 371–396, 1996.

[14] Ueber, S.J, Die Theorie der Eisbildung, insbesondere über die Eisbildung im Polarmeer, *Ann. Phys. Chem.*, **4**, pp. 269-286, 1891.

[15] Neumann F., *In Die partiellen Differentialgleichungen der Phvsik. Vol. 2*, Vieweg, Braunschweig, 1912.

[16] Tarzia D.A., Exact solution for a Stefan problem with convective boundary condition and density jump, *Proc. Appl. Math. Mech.*, **7**, pp. 1040307–1040308, 2007.

[17] Egolf P.W. & Manz H., Theory and modeling of phase change materials with and without mushy regions, *Int. J. Heat Mass Transfer*, **31**, pp. 2917-2924, 1994.

[18] Hollmüller P., Analytical characterization of amplitude-dampening and phase-shifting in air/soil heat-exchangers, *Int. J. Heat and Mass Transfer*, **46**, pp. 4303–4317, 2003.

[19] Origgi D. on behalf of BASF AG, Influence of Thermal Insulation and Phase-Change Material on Energy Demand and CO_2-Emissions in Different European Climates, Darmstadt, Germany, 2006.